Supporting Information for:

Electrochemical study of a nonheme Fe(II) complex in the presence of dioxygen. Insights into the reductive activation of O_2 at Fe(II) centers.

Nathalie Ségaud, Elodie Anxolabéhère-Mallart, Katell Sénéchal-David, Laura Acosta-Rueda, Marc Robert, Frédéric Banse.

Materials, synthetic procedures and physical measurements.

All moisture and oxygen sensitive compounds were prepared using standard high vacuum line, Schlenk and cannula techniques. All reagents were purchased from Aldrich or Acros and used as received unless noted otherwise. Acetonitrile solvent for spectroscopic measurements was purified by distillation, under argon, over CaH_2. For electrochemical experiments, extra dry acetonitrile was passed over alumina before use. Electrolytic solutions were prepared by using recrystallized tetrabutylammonium hexafluorophosphate. The ligand TPEN (N,N,N',N'-tetrakis(2-pyridylmethyl)ethane-1,2-diamine) and the complex $[(TPEN)Fe^{II}](PF_6)_2$ (**1**) were obtained following a previously reported procedure.[1] This latter was recrystallized in acetonitrile by vapour diffusion of *tert*-butylmethylether to give $[(TPEN)Fe^{II}](PF_6)_2$; H_2O; 2 CH_3CN, as determined by X-ray diffraction.[2] Complex **2** was isolated as $[(TPEN)Fe^{III}(OOH)](PF_6)_2$ following a procedure previously reported for a related compound,[3] and described hereafter. To a methanol solution of precursor **1** at room temperature was added 100 eq. H_2O_2 to immediately yield the purple complex **2**. Then, the solution was cooled down to -80°C and 10 eq. $NaPF_6$ and cold diethylether were added to precipitate the purple solid. The powder was carefully washed with diethylether, then dissolved in the minimum volume of butyronitrile at -80°C. The concentration in $Fe^{III}(OOH)$ was determined by UV-visible spectrophotometry. This so-called stock solution was used for further experiments. Formation of complex **3** from the stock solution diluted in acetonitrile was performed at -40°C upon addition of 5 eq. NEt_3. ***UV-Visible*** studies were performed using a Varian CARY 50 spectrophotometer equipped with a Hellma immersion probe with optic fibers. The temperature was controlled using a Thermo Haake CT90L cryostat.

X-band EPR spectra were recorded on frozen solutions using a Bruker Elexsys 500E spectrometer at 100K or 5K. ***Cyclic Voltammetry*** experiments were performed using an Autolab potentiostat. The electrolyte salt (Bu_4NPF_6) was recrystallized and all the glassware was dried at 110°C before use. All the cyclic voltammograms (CVs) were recorded from acetonitrile solution containing 0.1 M Bu_4NPF_6 at a scan rate of 0.1 V/S. Study of the reaction between complex **1** and O_2 were performed in air saturated acetonitrile at room temperature, *i.e.* at a dioxygen concentration of 1.62 mM.[4] ***Simulations of the CVs*** were obtained using Digielch program.[5] The electrochemical parameters of O_2 and $[(TPEN)Fe^{II}]^{2+}$ were first obtained separately before analysing the $\{O_2 + [(TPEN)Fe^{II}]^{2+}]\}$ system.

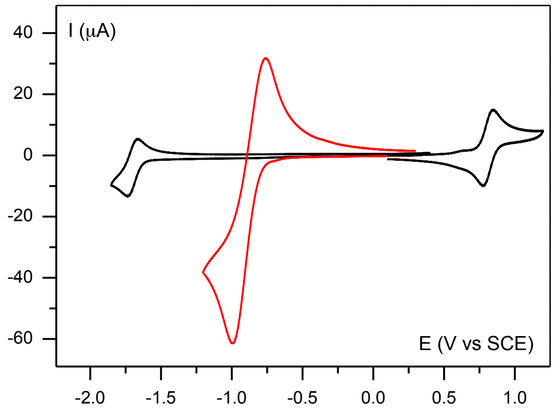

Figure S1. *CV of O_2 1.62 mM (red) and **1** (black) 0.88 mM under argon Experimental conditions: dry CH_3CN + 0.1 M $TBAClO_4$ T = 20°C, v=0.1 V s^{-1}.*

*This figure clearly shows that the Fe(II)/Fe(I) (E^0 = -1.70 V vs SCE) reduction wave of **1** occurs at lower potential than the $O_2/O_2^{\circ-}$ one (E^0 = -0.87 V vs SCE). Thus, reaction between Fe(I) and $O_2^{\circ-}$ has not to be taken into account in this study.*

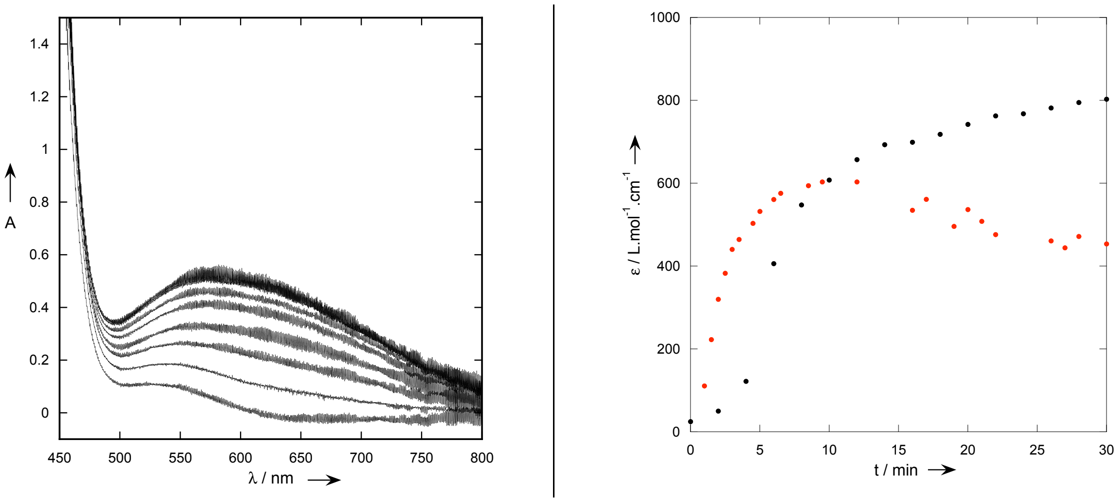

Figure S2. *(Left) UV-visible evolution of* $[(TPEN)Fe^{II}]^{2+}$ *(**1**) (0.75 mM) in the presence of 1 eq.* BPh_4^- *and 1 eq.* $HClO_4$ *in a dioxygen saturated acetonitrile at -20°C. (Right) Time trace at 650 nm for the reaction of* $[(TPEN)Fe^{II}]^{2+}$ *(**1**) with* O_2 *in the presence of 1 eq. of both* BPh_4^- *and* $HClO_4$ *(red dots) and of* $[(L_5^2aH)Fe^{II}]^{2+}$ *with* O_2 *in the presence of 2 eq. of* BPh_4^- *and* $HClO_4$ *(black dots).*

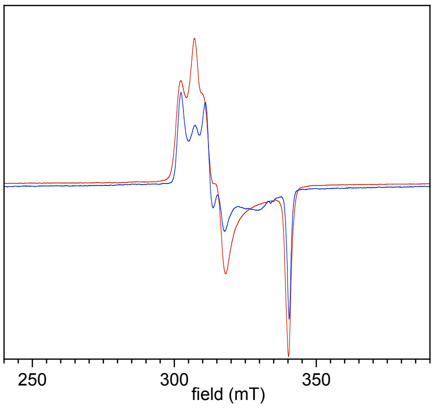

Figure S3. *X-band EPR spectrum at 100 K of* $[(TPEN)Fe^{III}(OOH)]^{2+}$ *(**2**) generated by reaction of **1** with 50 eq* H_2O_2 *in the presence of 2 eq of* $HClO_4$ *(red) or isolated as its* PF_6^- *salt and redissolved in butyronitrile (blue).*

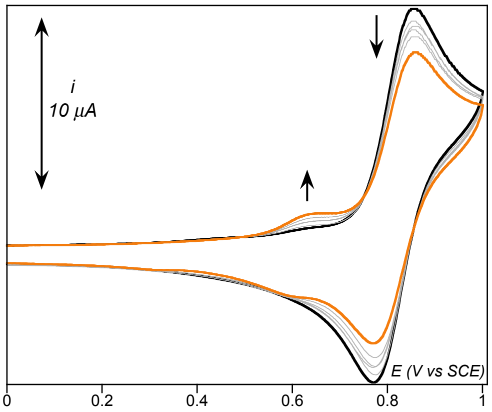

Figure S4. *CVs at a glassy carbon electrode of **1** (0.8 mM) at a scan rate of 0.1 V/s in aerated acetonitrile (1.62 mM in O_2) at RT, and evolution upon addition of water up to a concentration of 0.22 M (orange trace). Peak at $E_{p,a}$ = 0.85 V (oxidation of **1** $[(TPEN)Fe^{II}]^{2+}$) decreases concomitantly with the increase of a new plateau shaped feature at ca. 0.62 V attributed to the oxidation of $[(TPEN)Fe^{II}(OH_2)]^{2+}$ (see figure S12 for CV simulation). Note that the potential values are slightly different than the one reported on figure 1 due to differences in temperature.*

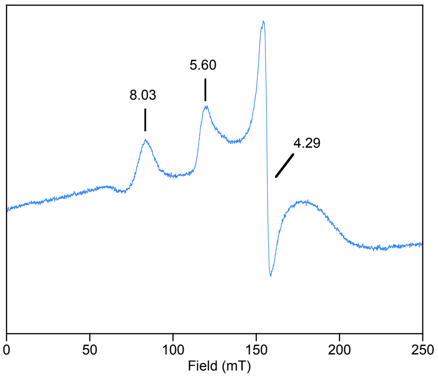

Figure S5. *X-band EPR at 10 K of a solution of **3** (signals at g = 8.03 and g = 5.60) resulting from addition of 5 eq. NEt_3 to acetonitrile solution of **2** at -40°C. The signal at g = 4.29 corresponds to ubiquitous HS (S=5/2) Fe^{III}.*

CV analysis for CV simulations.

Glossary of symbols

$D_{species}$ = diffusion coefficient of the subscript species

E^0_{couple} = standard potential of the subscript couple

k_s = rate constant of the heterogeneous electron transfer

α = transfer coefficient of the electron transfer

1- O_2 electrochemical characterization in CH_3CN

O_2 in dry CH_3CN leads to a one electron reversible wave. Simulation of this wave allows evaluating the following parameters taking into account that the electrode surface is 0.07 cm²: $E^0_{O_2/O_2^{\bullet-}} = -0.87$ V *vs* SCE, $k_S(O_2/O_2^{\bullet-}) = 0.0045$ cm/s (taking α = 0.5) and $D_{O_2} = D_{O_2^{\bullet-}} = 9\times10^{-5}$ cm²/s (figure S6). These values parameters are slightly different to those published in the literature.[6]

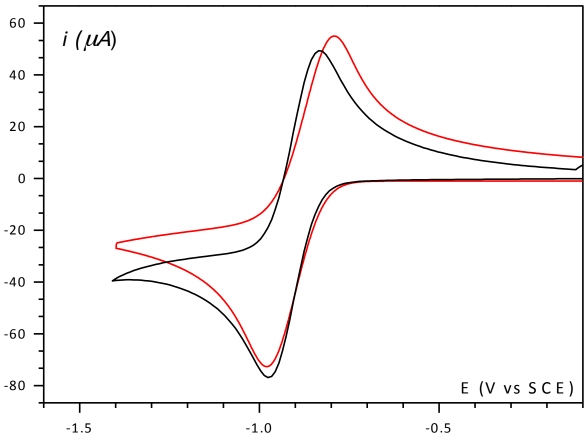

Figure S6. *(black) CV of O_2 in CH_3CN with 0.1 M $TBAPF_6$ saturated with air (1.62 mM O_2)[4] at 0.1 V/s at a glassy carbon disk electrode at 293 K. (red) Simulation with $E^0_{O_2/O_2^{\bullet-}} = -0.87$ V vs. SCE, $k_S(O_2/O_2^{\bullet-}) = 0.0045$ cm/s and $D_{O_2} = D_{O_2^{\bullet-}} = 9\times10^{-5}$ cm²/s.*

2- $[(TPEN)Fe^{II}]^{2+}$ electrochemical characterization in CH_3CN

Cyclic voltammetry of $[(TPEN)Fe^{II}]^{2+}$ complex **1** leads to a quasi-reversible oxidation wave (figure S7). Simulation of this wave assuming a simple one electron Fe^{III} / Fe^{II} conversion leads to the following parameters $E^0_{Fe^{III}/Fe^{II}} = 0.81$ V vs. SCE, $k_S(Fe^{III}/Fe^{II}) = 0.0095$ cm/s (taking α = 0.5) and $D_{Fe^{II}} = D_{Fe^{III}} = 1\times10^{-5}$ cm^2/s.

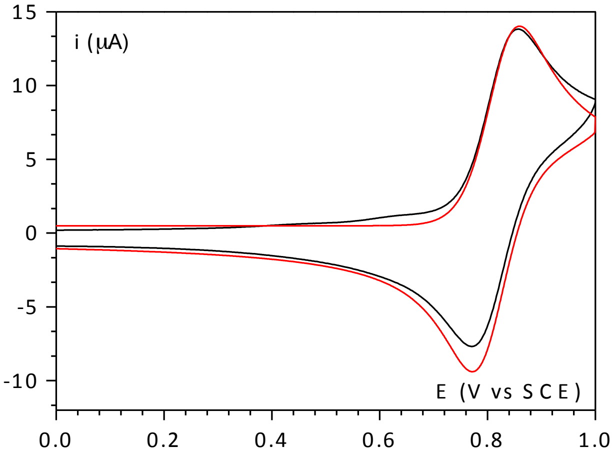

Figure S7. *(black) CV of **1** (0.81 mM) in CH_3CN with 0.1 M Bu_4NPF_6 at 0.1 V/s at a glassy carbon disk electrode at 293 K. (red) Simulation with* $E^0_{Fe^{III}/Fe^{II}} = 0.81$ *V vs. SCE,* $k_S(Fe^{III}/Fe^{II}) = 0.0095$ *cm/s and* $D_{Fe^{II}} = D_{Fe^{III}} = 1\times10^{-5}$ *cm^2/s.*

Table S1. Parameters obtained from simulations of the CVs of the O_2 to $O_2^{\bullet-}$ reduction and $[(TPEN)Fe^{II}]^{2+}$ to $[(TPEN)Fe^{III}]^{3+}$ oxidation, at 293 K.

	$O_2/O_2^{\bullet-}$	$[(TPEN)Fe^{III}]^{3+}/[(TPEN)Fe^{II}]^{2+}$
***E*° (V vs. SCE)**	-0.87	0.81
k_S (cm s^{-1})	4.5×10^{-3}	9.5×10^{-3}
***D* (cm^2 s^{-1})**	9×10^{-5}	1×10^{-5}

3 - Electrochemical characterization of intermediate $[(TPEN)Fe^{IV}(O)]^{2+}$ (4)

Simulation of CVs of **1** recorded at 0°C was first executed in order to obtain the diffusion coefficient value for complexes at 0°C. A value of $D_{Fe} = 3 \times 10^{-6}$ cm²/s was obtained.

CVs of **4** in CH_3CN were then simulated according to Scheme S1. Results are shown on Figure S8. The first reaction corresponds to the 1 electron reduction of **4** $[(TPEN)Fe^{IV}(O)]^{2+}$ into $[(TPEN)Fe^{III}(O)]^{+}$. The second reaction is the acid / base reaction between the latter $[(TPEN)Fe^{III}(O)]^{+}$ and $[(TPEN)Fe^{III}(OH)]^{2+}$. The last reaction corresponds to the 1 electron reduction of $[(TPEN)Fe^{III}(OH)]^{2+}$ to yield $[(TPEN)Fe^{II}(OH)]^{+}$.

Scheme S1

$$\textbf{E} \quad \underset{\textbf{(4)}}{[(TPEN)Fe^{IV}(O)]^{2+}} + e^- \xrightleftharpoons{E^0,\ k_S} [(TPEN)Fe^{III}(O)]^{+}$$

$$\textbf{C} \quad [(TPEN)Fe^{III}(O)]^{+} + H_2O \xrightleftharpoons{K,\ k_f,\ k_b} [(TPEN)Fe^{III}(OH)]^{2+} + OH^-$$

$$\textbf{E} \quad [(TPEN)Fe^{III}(OH)]^{2+} + e^- \xrightleftharpoons{E^0,\ k_S} [(TPEN)Fe^{II}(OH)]^{+}$$

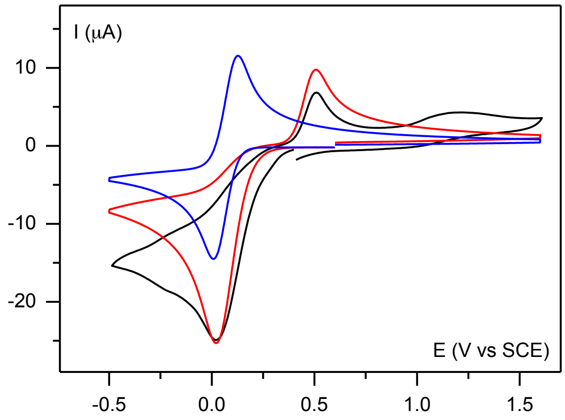

Figure S8. *(black) CV of* ***4*** *(1.5 mM) in* CH_3CN *with 0.1 M* Bu_4NPF_6 *at 0.1 V/s at a glassy carbon disk electrode at 273 K. (red) Simulation according to scheme S1 with* $E^0_{Fe^{IV}(O)/Fe^{III}(O)}$ *= 0.07 V vs SCE,* $E^0_{Fe^{III}(OH)/Fe^{II}(OH)}$ *= 0.45 V vs SCE;* $k_S(Fe^{IV}(O)/Fe^{III}(O)) = 0.0025$ *cm/s and* $k_S(Fe^{III}(OH)/Fe^{II}(OH)) = 0.0025$ *cm/s;* $D_{Fe} = 3 \times 10^{-6}$ *cm²/s,* $K = 1 \times 10^5\ M^{-1}$ *and* $k_f = 1 \times 10^8\ M^{-1}s^{-1}$ *and* $[H_2O]$*= 1.5 mM; (blue) simulation according to scheme S1, with* $[H_2O]$*= 0 mM.*

The value of $E^0_{Fe^{IV}(O)/Fe^{III}(O)}$ was taken as slightly more positive than the experimental peak potential E_p = 0.0195 V *vs* SCE. Simulations obtained according to a scheme which do not include the chemical reaction (protonation fo Fe^{III}(O)) leads to a 1 electron oxidation wave centered at $E^0_{Fe^{IV}(O)/Fe^{III}(O)}$ (figure S8, blue trace). We hypothesized that the [(TPEN)Fe^{III}(O)]$^+$ species is basic enough to be easily protonated in acetonitrile containing 1.5 mM of water (the content of water in dry acetonitrile was taken equimolar to the complex **1** concentration) and 1.2 eq H$^+$ v*s* **1** arising from mCPBA. Therefore the chemical reaction was considered favourable ($K = 1\times10^8$) and the kinetic constant was chosen fast ($k_f = 1\times10^8$ M^{-1}s^{-1}).

The simulation shown on figure S8 supports the validity of Scheme S1. The values of K and k_f parameters could be adjusted in order to improve the fitting of the experimental curve. Nevertheless, the chemical instability of species **4** and [(TPEN)Fe^{III}(O)]$^+$ species precludes the experimental access to the $E^0_{Fe^{IV}(O)/Fe^{III}(O)}$ value. Therefore, it is not possible to fix the $E^0_{Fe^{IV}(O)/Fe^{III}(O)}$ value in the simulation process, thus rendering impossible the exact determination of the kinetic parameters.

4- Electrochemical characterization of intermediate [(TPEN)Fe^{III}(OOH)]$^{2+}$ (2)

CVs of **2** were simulated according to Scheme S2. The first reaction is the 1 electron reduction of **2** to yield [(TPEN)Fe^{II}(OOH)]$^+$. The second reaction corresponds to the transformation of the latter unidentified intermediate. It is hypothesized that Fe(II)OOH is unstable. Therefore, we propose that [(TPEN)Fe^{II}(OOH)]$^+$ readily yields [(TPEN)Fe^{II}]$^{2+}$ (**1**) which is stable under such reductive conditions. Note that the chemical reaction has not been balanced for simplification. A mechanism involving O-O cleavage upon the one electron reduction of **2** (to yield **4** and OH$^-$) would lead to an overall 3 electrons reduction as **4** undergoes a 2 electrons reduction process. Such a scenario is not compatible with the intensity of the cathodic process observed for **2**.

Scheme S2.

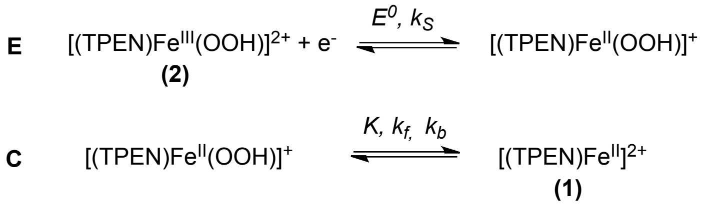

$$\textbf{E}\quad [(\mathrm{TPEN})\mathrm{Fe^{III}(OOH)}]^{2+} + e^- \xrightleftharpoons{E^0,\ k_S} [(\mathrm{TPEN})\mathrm{Fe^{II}(OOH)}]^{+}$$

(2)

$$\textbf{C}\quad [(\mathrm{TPEN})\mathrm{Fe^{II}(OOH)}]^{+} \xrightleftharpoons{K,\ k_f,\ k_b} [(\mathrm{TPEN})\mathrm{Fe^{II}}]^{2+}$$

(1)

Diffusion coefficients values for all Fe complexes were taken as $D_{Fe} = 1\times10^{-6}$ cm^2/s according to the value estimated from the simulation of one electron oxidation process of **1** recorded at -40°C**.** The value of $E^0_{Fe^{III}(OOH)/Fe^{II}(OOH)}$ was taken as slightly more negative than the peak potential experimentally measured. The k_S values was taken as identical to the one of complex **1** ($k_S(Fe^{III}/Fe^{II}) = 0.0095$ cm^2/s) at 293K. The equilibrium between Fe(II)OOH and Fe(II) is in favour of Fe(II) formation ($K = 1\times10^8$ M^{-1})

and fast $k_f = 1\times10^8$ $M^{-1}s^{-1}$). Based on these hypotheses, a simulation of CV of **2** is shown in figure S9 (red trace).

Experimental CV can also be nicely fitted (blue trace) using a simulation according to the following electrochemical reaction, with a slower electron transfer (Scheme S3). This reaction is a simplified version of the mechanism depicted in Scheme S2, and is the one used for the final simulation (Scheme S6).

Scheme S3.

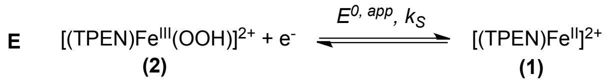

$$\mathbf{E} \quad \underset{\mathbf{(2)}}{[(TPEN)Fe^{III}(OOH)]^{2+}} + e^- \xrightleftharpoons{E^{0,\,app},\ k_S} \underset{\mathbf{(1)}}{[(TPEN)Fe^{II}]^{2+}}$$

where $E^{0,\,app}_{Fe^{III}(OOH)/Fe^{II}}$ is defined as the potential of the Fe^{III}(OOH)/Fe^{II} couple ($E^{0,\,app}_{Fe^{III}(OOH)/Fe^{II}}$ = -0.14 V vs SCE and $k_S(Fe^{III}(OOH)/Fe^{II}) = 0.0045$ cm^2/s).

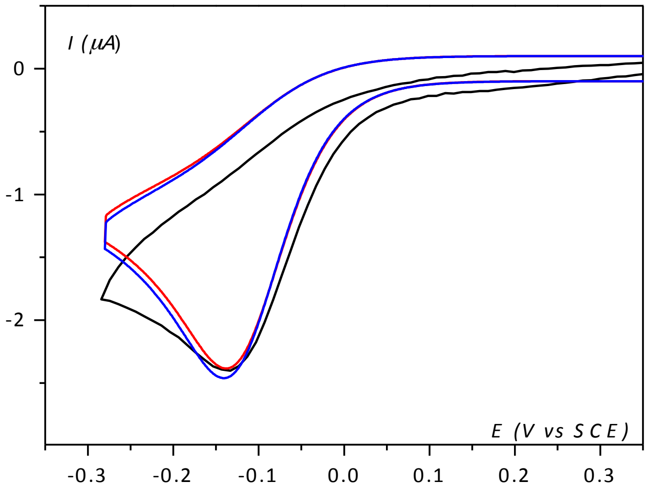

Figure S9. *(black) CV of **2** (0.34 mM) in CH_3CN with 0.1 M Bu_4NPF_6 at 0.1 V/s at a glassy carbon disk electrode at 233 K. (red) Simulation according to scheme S2 with* $E^0_{Fe^{III}(OOH)/Fe^{II}(OOH)}$ *= -0.17 V vs SCE,* $k_S(Fe^{III}(OOH)/Fe^{II}(OOH)) = 0.0095$ *cm/s and* $D_{Fe^{II}} = D_{Fe^{III}} = 1\times10^{-6}$ cm^2/s, $K = 1\times10^8$ M^{-1} *and* $k_f = 1\times10^8$ $M^{-1}s^{-1}$. *(blue) Simulation according to equation in Scheme S3 (* $E^{0,\,app}_{Fe^{III}(OOH)/Fe^{II}}$ *= -0.14 V vs SCE and* $k_S(Fe^{III}(OOH)/Fe^{II}) = 0.0045$ *cm/s).*

5- CV of the {O_2 + $[(TPEN)Fe^{II}]^{2+}$ (1)} system in CH_3CN.

a/ {O_2 + 1} system

Simulation of the experimental CV were obtained through successive steps. We first modeled the experimental data according to a square scheme (upper left square in scheme S5 and scheme 4 in manuscript) including a CE and EC mechanisms. Simulations have been performed using the parameters determined above for $O_2/O_2^{\bullet-}$ couple and $[(TPEN)Fe^{II}]^{2+}$ **1** (Table S1). Diffusion coefficient for all the Fe species were taken as equal to the one of **1**, $D_{Fe^{II}} = D_{Fe^{III}} = 1\times10^{-5}\ cm^2/s$. The K and k_f values for the equilibrium between $[(TPEN)Fe^{II}]^{2+}$ and O_2 (reaction C1 in scheme S6) were determined from simulation of the oxidation wave of $[(TPEN)Fe^{II}]^{2+}$ in O_2 saturated solution (see part **b/** below). It is observed that the new feature at *ca.* -0.8 V *vs* SCE can be modeled only provided the CE pathway is considered. The $[(TPEN)Fe^{II}O_2^{\bullet-}]^+$ (**1-$O_2^{\bullet-}$**) then obtained readily evolves to yield its valence tautomer $[(TPEN)Fe^{III}(OO)]^+$ (**3**) (reaction C3 in scheme S6), which has been spectroscopically characterized (see manuscript).

We then added reactions that consume $[(TPEN)Fe^{III}(OO)]^+$ **3** based on the following experimental observations *(i)* $[(TPEN)Fe^{III}(OO)]^+$ **3** is reduced at a less negative potential (*ca.* -0.6 V *vs.* SCE), *(ii)* an acid/base equilibrium between **3** and $[(TPEN)Fe^{III}(OOH)]^{2+}$ (**2**) exists according to Scheme S4, *(iii)* (**2**) is reduced irreversibly at -0.14 V vs SCE (see simulation above).

Scheme S4

$$[(TPEN)Fe^{III}(OO)]^+ + H_2O \underset{k_b}{\overset{K,k_f}{\rightleftharpoons}} [(TPEN)Fe^{III}(OOH)]^{2+} + HO^-$$

Thus we introduce a second square scheme that includes various paths for the consumption of $[(TPEN)Fe^{III}(OO)]^+$ as depicted below (Scheme S5).

Scheme S5. *Proposed reduction mechanism considered to model the experimental CVs for the reaction between O_2 and complex **1**. The ligand has been omitted for clarity.*

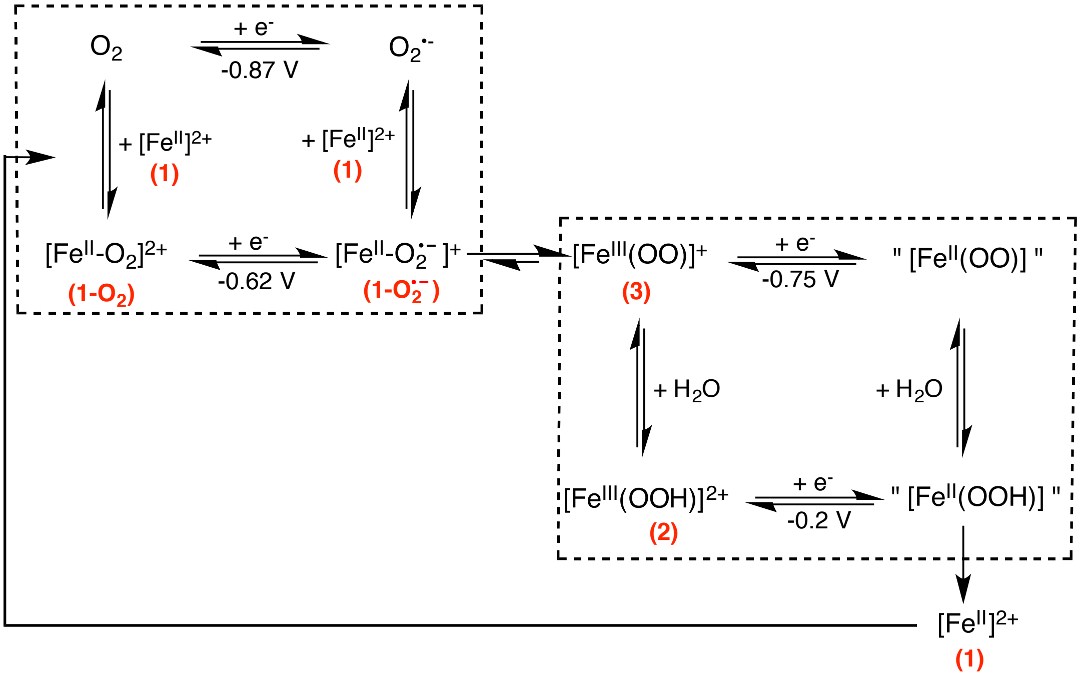

Additionally, it is observed that in order to reproduce the anodic features satisfactorily, *(i)* regeneration of $[(TPEN)Fe^{II}]^{2+}$ **1** (reactions E4, C4 and C5 in scheme S6) and *(ii)* oxidation of the $[(TPEN)Fe^{III}(OO)]^{2+}$ **3** species have to be taken into account (reaction E6 in scheme S6). Thus, we propose that consumption of $[(TPEN)Fe^{III}(OO)]^{+}$ ultimately regenerates $[(TPEN)Fe^{II}]^{2+}$ **(1)**. Figure S10 compares various cases.

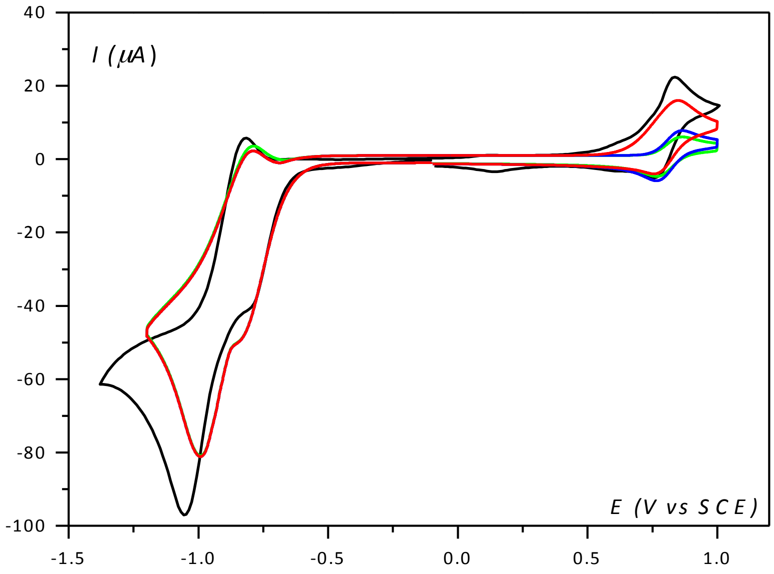

Figure S10. *(black) CV of **1** (1.58 mM) in the presence of O_2 (1.62 mM) in CH_3CN with 0.1 M Bu_4NPF_6 at 0.1 V/s at a glassy carbon disk electrode at room temperature. (Green) Simulation for which **1** is not regenerated and oxidation of **3** is not considered. (Blue) simulation for which **1** is regenerated and oxidation of **3** is not considered. (Red) Simulation taking into accounts both the regeneration of **1** and the oxidation of **3**. The parameters used are the one given in Scheme S6.*

Finally, the CV of O_2 in presence of increasing amounts of **1** and different amounts of water is satisfactorily modeled with the following mechanism and parameters. Note that the diffusion coefficient of all the Fe species were taken as equal to the one of **1** : $D_{Fe^{II}} = D_{Fe^{III}} = 1\times10^{-5}$ cm^2/s.

Scheme S6. *parameters used to simulate the CV of O_2 in presence of increasing amounts of **1** and different amounts of water. The ligand TPEN has been omitted for clarity.*

E1	$O_2 + e^- \rightleftharpoons O_2^{\bullet-}$	$E^0 = -0.87\ V,\ k_s = 0.0045\ cm/s$
C1	$O_2 + \underset{(1)}{[Fe^{II}]^{2+}} \rightleftharpoons \underset{(1\text{-}O_2)}{[Fe^{II}\text{-}O_2]^{2+}}$	$K = 30\ M^{-1},\ k_f = 10^6\ M^{-1}.s^{-1}$
C2	$O_2^{\bullet-} + \underset{(1)}{[Fe^{II}]^{2+}} \rightleftharpoons \underset{(1\text{-}O_2^{\bullet-})}{[Fe^{II}\text{-}O_2^{\bullet-}]^{+}}$	$K = 5\ 10^5\ M^{-1},\ k_f = 10^8\ M^{-1}.s^{-1}$
C3	$\underset{(1\text{-}O_2^{\bullet-})}{[Fe^{II}\text{-}O_2^{\bullet-}]^{+}} \rightleftharpoons \underset{(3)}{[Fe^{III}(OO)]^{+}}$	$K = 1\ 10^{10}\ M^{-1},\ k_f = 10^{10}\ M^{-1}.s^{-1}$
E2	$\underset{(1\text{-}O_2)}{[Fe^{II}\text{-}O_2]^{2+}} + e^- \rightleftharpoons \underset{(1\text{-}O_2)}{[Fe^{II}\text{-}O_2^{\bullet-}]^{+}}$	$E^0 = -0.62\ V,\ k_s = 0.009\ cm/s$
E3	$\underset{(3)}{[Fe^{III}(OO)]^{+}} + e^- \rightleftharpoons [Fe^{II}(OO)]$	$E^0 = -0.75\ V,\ k_s = 0.0045\ cm/s$
C4	$\underset{(3)}{[Fe^{III}(OO)]^{+}} + H_2O \rightleftharpoons \underset{(2)}{[Fe^{III}(OOH)]^{2+}}$	$K = 0.35\ M^{-1},\ k_f = 10\ M^{-1}.s^{-1}$
C5	$[Fe^{II}(OO)] + H_2O \rightarrow [Fe^{II}]^{2+}$	$K = 7\ 10^8\ M^{-1},\ k_f = 0.1\ M^{-1}.s^{-1}$
E4	$[Fe^{III}(OOH)]^{2+} + e^- \rightleftharpoons \underset{(1)}{[Fe^{II}]^{2+}}$	$E^0 = -0.2\ V,\ k_s = 0.0045\ cm/s$
E5	$[Fe^{III}]^{3+} + e^- \rightleftharpoons \underset{(1)}{[Fe^{II}]^{2+}}$	$E^0 = 0.81\ V,\ k_s = 0.009\ cm/s$
E6	$"[Fe^{III}(OO)]^{2+}{}_{ox}" + e^- \rightleftharpoons \underset{(3)}{[Fe^{III}(OO)]^{+}}$	$E^0 = 0.75\ V,\ k_s = 0.0045\ cm/s$
E7	$[Fe^{III}(OH_2)]^{3+} + e^- \rightleftharpoons [Fe^{II}(OH_2)]^{2+}$	$E^0 = 0.62\ V,\ k_s = 0.009\ cm/s$
C6	$\underset{(1)}{[Fe^{II}]^{2+}} + H_2O \rightleftharpoons [Fe^{II}(OH_2)]^{2+}$	$K = 1\ M^{-1},\ k_f = 0.1\ M^{-1}.s^{-1}$
C7	$[Fe^{III}]^{3+} + H_2O \rightleftharpoons [Fe^{III}(OH_2)]^{3+}$	$K = 1757\ M^{-1},\ k_f = 1\ 10^{-15}\ M^{-1}.s^{-1}$

b/ simulation of the oxidation wave of $[(TPEN)Fe^{II}]^{2+}$ (1) in O_2 saturated solution

Experimental CV was modeled according to the CE mechanism depicted in Scheme S7. With a fixed k_f value of 10^6 $M^{-1}s^{-1}$ (rapid), K can be varied up to K= 30 M^{-1}, without changing the shape of the wave (Figure S11).

Scheme S7

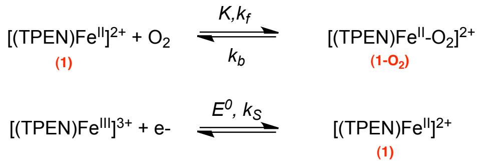

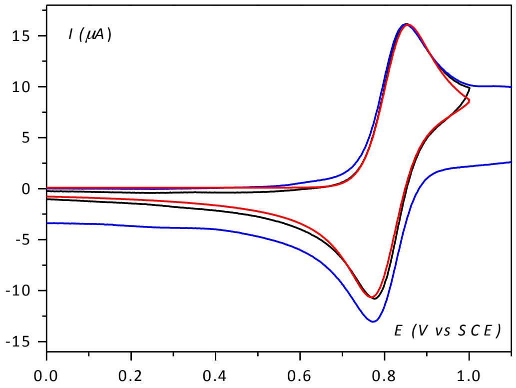

Figure S11. *CV at a glassy carbon disk electrode of* ***1*** *(0.9 mM) in CH_3CN solution with 0.1 M Bu_4NPF_6 under argon (black trace), saturated with air (1.62 mM O_2) (blue trace) and simulation according to scheme S7 with parameters given in scheme S6 (red trace). Experimental conditions: v=0.1 V/s and T= 273 K. The samples were initially scanned towards positive potentials.*

c/ simulation of the oxidation wave of $[(TPEN)Fe^{II}]^{2+}$ (1) in presence of water

The kinetic and equilibrium constants for equilibrium between $[(TPEN)Fe^{II}]^{2+}$ (**1**) and $[(TPEN)Fe^{II}(OH_2)]^{2+}$ were estimated from simulation of the Fe(II)/Fe(III) oxidation process of a 1.54 mM solution of $[(TPEN)Fe^{II}]^{2+}$ in the presence of increasing amounts of water according to Scheme S8 (Figure S12).

Scheme S8

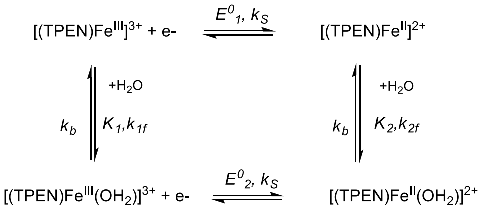

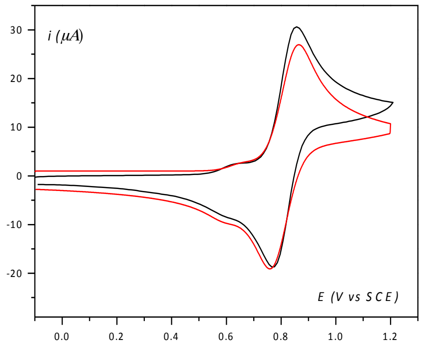

Figure S12. *CV at a glassy carbon disk electrode of* ***1*** *(1.54 mM) in CH3CN solution with 0.1 M Bu_4NPF_6 under argon (black trace) in presence of 0.1 M of water and simulation according to scheme S8 with the parameters given in scheme S6 (red trace). Experimental conditions: v=0.1 V/s and T= 273 K.*

All the numerical values given above are not to be misunderstood as values determined by fitting but rather as one set of numerical values consistent with the many complex features of the observed CVs. In the case of E3 and E4 (Scheme S6), the experimental peak potentials were used as starting values for the simulations. Determination of standard potentials for these reactions would require further experiments. However, the simulations based on the above parameters support the validity of the mechanism shown in Scheme S5.

References

(1) Chang, H. R.; Mccusker, J. K.; Toftlund, H.; Wilson, S. R.; Trautwein, A. X.; Winkler, H.; Hendrickson, D. N. *J. Am. Chem. Soc.* **1990**, *112*, 6814.

(2) Ségaud, N.; Sénéchal-David, K.; Banse, F.; Guillot, R., (2014) Private communication to the Cambridge Structural Database, deposition number CCDC 984727.

(3) a) Martinho, M.; Dorlet, P.; Rivière, E.; Thibon, A.; Ribal, C.; Banse, F.; Girerd, J.-J. *Chem. Eur. J.* **2008**, *14*, 3182; b) Thibon, A.; Jollet, V.; Ribal, C.; Sénéchal-David, K.; Billon, L.; Sorokin, A. B.; Banse, F. *Chem. Eur. J.* **2012**, *18*, 2715.

(4) Achord, J. M.; Hussey, C. L. *Anal. Chem.* **1980**, 601.

(5) Rudolph, M. *Journal of Electroanalytical Chemistry* **2003**, *543*, 23.

(6) Vasudevan, D.; Wendt, H. *Journal of Electroanalytical Chemistry* **1995**, *392*, 69.